Journal of Solid State Chemistry **151,** 260–266 (2000)
doi:10.1006/jssc.2000.8649, available online at http://www.idealibrary.com on IDEAL®

Incommensurate Cu/Co Ordering in the $TlCo_{2-x}Cu_xSe_2$ ($x \sim 1$) System

L. Norén,* R. L. Withers,* and R. Berger†

*Research School of Chemistry, Australian National University, Canberra, ACT, 0200 Australia and †Department of Inorganic Chemistry, Uppsala University, Box 538, SE-751 21 Uppsala, Sweden

Received November 12, 1999; in revised form February 3, 2000; accepted February 10, 2000

Cu/Co ordering in $TlCo_{2-x}Cu_xSe_2$, ($x \sim 1$) has been investigated using electron and X-ray powder diffraction. The average structure of the $x = 1$ compound can be indexed on an *F*-centered orthorhombic cell, $a = 5.5518(6)$ Å, $b = 5.4755(5)$ Å, and $c = 13.7387(17)$ Å. Additional weak satellite reflections characterized by the primary modulation wave vector $\mathbf{q}_i \sim 0.184\mathbf{a}^*$ and indicative of an incommensurate modulated structure are revealed by electron diffraction. Characteristic extinction conditions in conjunction with *mmm* Laue symmetry and known crystal chemical constraints imply a (3 + 1)-dimensional superspace group symmetry of $Fmmm(\alpha 01)00s$. The incommensurate modulation is attributed to occupational ordering of the two transition metal atoms and associated structural relaxation. The real space interpretation of the Cu/Co ordering pattern is that copper and cobalt atoms form separate layers in the structure at $z = \frac{1}{4}$ and $\frac{3}{4}$, respectively. These layers are periodically interchanged as one moves along the *x* direction. Two periods of this square-wave-like modulation is close to 11a in length but is non-rational compared with the average structure. © 2000 Academic Press

Key Words: **thallium cobalt copper selenide; incommensurate modulated structure; electron diffraction; Cu/Co ordering.**

1. INTRODUCTION

Many ternary transition metal chalcogenides of stoichiometry AM_2X_2 (A = K, Rb, Cs or Tl; M is a transition metal; and $X = S$, Se, or Te) crystallize in the tetragonal $ThCr_2Si_2$ structure type (space group $I4/mmm$). These compounds have been intensively studied recently, partly as a result of their intriguing two-dimensional electronic and magnetic properties (1–7). Most are highly metallic conductors with low-temperature magnetic properties that are strongly dependent upon the metal composition. $TlCo_2Se_2$, for example, is antiferromagnetic, and KCo_2Se_2 ferromagnetic, while $TlCu_2Se_2$ is paramagnetic (1–7).

The ideal $ThCr_2Si_2$ structure type consists of infinite layers of edge-sharing MX_4 tetrahedra (half a unit cell thick [001] layers of anti-fluorite type) forming $[M_2X_2]^{-1}$ sheet-like anions separated in turn by layers of A cations (see Fig. 1). The A cations are located in position 2*a* (000) and are 8 coordinated by the chalcogenide X ions in 4*e* (00z, $z \sim 0.36$). The A–X distance is close to the sum of the ionic radii of A and X while the M atoms in position 4*d* (0, $\frac{1}{2}$, $\frac{1}{4}$) form more covalent bonds to the X atoms. The distance between the two MX_4 sheets is $c/2$, typically ~ 7 Å, so that the physical properties of these compounds have a strong two-dimensional character.

Substitution is possible on all three sites. Most attention, however, has focussed on substitution of the metal ions. The ability to substitute for both the A- and M-site ions in such structures gives rise to AM_2X_2–$A'M_2X_2$ and AM_2X_2–AM'_2X_2 pseudo-binary systems and the possibility of systematically investigating the dependence of the associated physical properties upon dopant ion type. Studies of this type have been carried out for a range of quaternary transition metal chalcogenides including $K_{1-x}Tl_xCo_2Se_2$ (3), $TlCu_{2-x}Fe_xSe_2$, $TlCu_{2-x}Al_xSe_2$, $TlCu_{2-x}Ga_xSe_2$ (4, 8), $TlCo_{2-x}Ni_xSe_2$ (2), and $TlCo_{2-x}Cu_xSe_2$ (4, 5). In virtually every case, continuous solid solutions (as indicated by unit cell dimensions) have been reported to exist between the two end members with no indication of metal ion ordering. In the case of the $TlCo_{2-x}Cu_xSe_2$ system, however, Berger and van Bruggen (4) reported that the diffraction lines of the original $I4/mmm$ tetragonal cell were split for the compound with a Cu content $x = 1$. In a more recent investigation, this splitting was also found for $x \geq 0.8$. The new diffraction lines are apparently well explained by an orthorhombic F-centred cell ($a = a_p - b_p$, $b = a_p + b_p$, $c = c_p$) based on the original tetragonal parent unit cell (5). The purpose of this paper is to investigate via electron diffraction the Cu/Co ordering underlying the reported line splitting in this $TlCo_{2-x}Cu_xSe_2$ ($x \sim 1$) system.

2. EXPERIMENTAL

2.1. Synthesis

Samples were prepared in a three-step process as follows. Thallium selenide, TlSe, was first fabricated by heating of the elements in a sealed Pyrex tube at 300°C. The ternary

0022-4596/00 $35.00

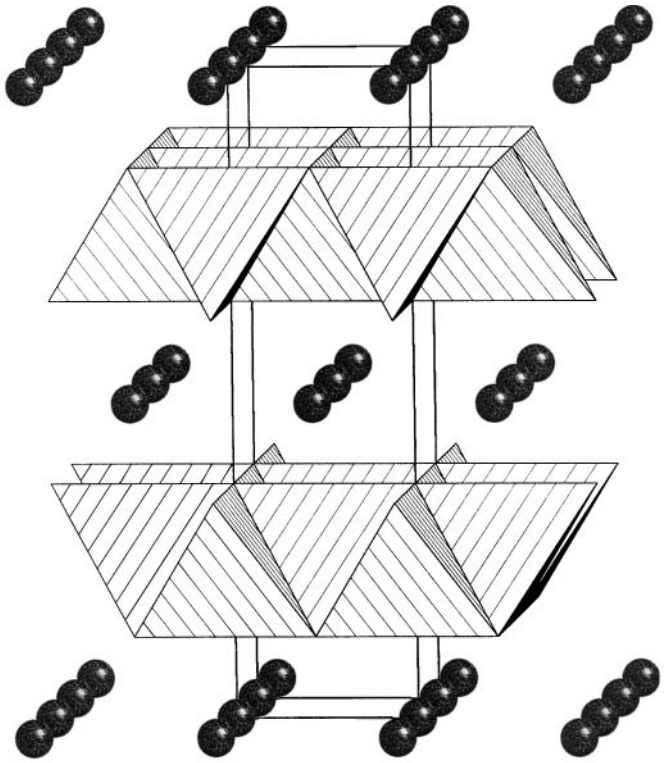

FIG. 1. Perspective drawing of the ideal $ThCr_2Si_2$ parent structure type ($I4/mmm$ space group symmetry, stoichiometry AM_2X_2) projected close to a $\langle 100 \rangle$ direction. The unit cell is outlined (the c direction is vertical). It consists of infinite layers of edge-sharing MX_4 tetrahedra (shaded) separated in turn by layers of A cations (the large dark balls).

compounds $TlCo_2Se_2$ and $TlCu_2Se_2$ were then synthesized by reacting stoichiometric amounts of TlSe, selenium, and the respective transition metal element. Finally, the quaternary transition metal chalcogenide samples were prepared by reacting stoichiometric amounts of the single-phase samples of $TlCo_2Se_2$ and $TlCu_2Se_2$ at 700°C in sealed silica tubes. The end product samples were black crystals that could easily be split into flakes, consistent with the layered nature of the compounds.

The end-member copper compound, $TlCu_2Se_2$, was synthesized at 400°C in an evacuated Pyrex tube. The reactants were ground, pelleted, and sintered until a homogeneous single-phase product was obtained as indicated by X-ray powder diffraction. The $TlCo_2Se_2$ was made via a silica tube synthesis. The reactants were never in contact with the glass walls but placed inside the tube in a cleaned alumina crucible in order to avoid reaction between cobalt and the silica in the tube walls. (At temperatures below 700°C this etching was not observed even for cobalt-rich samples). The sample was initially heated to 1000°C for two days and then kept at 800°C for a further week. A homogenization process similar to that described above for $TlCu_2Se_2$ (but at an annealing temperature of 800°C) was then conducted until no impurity phases could be detected.

2.2. Characterization

Specimens were examined by X-ray powder diffraction using a focusing Guinier-Hägg camera with monochromatized Cu$K\alpha_1$-radiation. For the accurate determination of unit cell dimensions, an internal standard of silicon (NBS No. 640) was added.

Specimens for electron microscopy were prepared by crushing and dispersing onto holey-carbon-coated copper grids. These grids were then examined with JEOL 100CX and Philips EM430 transmission electron microscopes (TEMs).

3. RESULTS

3.1. X-Ray Powder Diffraction

X-ray powder diffraction patterns confirmed a small orthorhombic splitting of the parent $I4/mmm$ diffraction lines in the case of $x \sim 1$ specimens. For $x = 1.0$ exactly, corresponding to the composition $TlCoCuSe_2$, the refined unit cell dimensions ($a = a_p - b_p$, $b = a_p + b_p$, $c = c_p$) were $a = 5.5517(6)$, $b = 5.4755(5)$, and $c = 13.739(2)$ Å and were consistent with an orthorhombic F-centered cell (5). The refined unit cell dimensions of the two tetragonal end-member phases were $a_p = 3.8468(4)$ and $c_p = 13.536(2)$ Å in the case of $TlCo_2Se_2$ and $a_p = 3.8574(2)$ and $c_p = 14.041(1)$ Å in the case of $TlCu_2Se_2$. Note the $\sim 3.7\%$ difference in c_p dimension but less than 0.3% increase in a_p dimension on going from the Co to the Cu compound. The c parameter of the 1:1 solid solution is consistent with the expectation from the point of view of Vegard's law.

As anticipated, disorder prevails at high temperatures so that orthorhombic splitting was absent for specimens rapidly quenched from 900°C.

3.2. Electron Diffraction

Careful measurement of [001] zone axis electron diffraction patterns (EDPs) of the $TlCoCuSe_2$ phase, such as that shown in Fig. 2(a), confirmed the orthorhombic splitting of the parent $I4/mmm$ diffraction lines. In addition, however, it also revealed the presence of weak additional incommensurate satellite reflections running along the **a*** (but not the **b***) direction of reciprocal space. Such an incommensurate modulation clearly distinguishes the **a*** (equivalent to the $[1\bar{1}0]_p^*$ direction of the original $I4/mmm$ parent unit cell) from the **b*** (equivalent to the $[110]_p^*$ direction of the original $I4/mmm$ parent unit cell) direction of reciprocal space and hence provides a rationale for the observed orthorhombic strain distortion of the parent tetragonal cell.

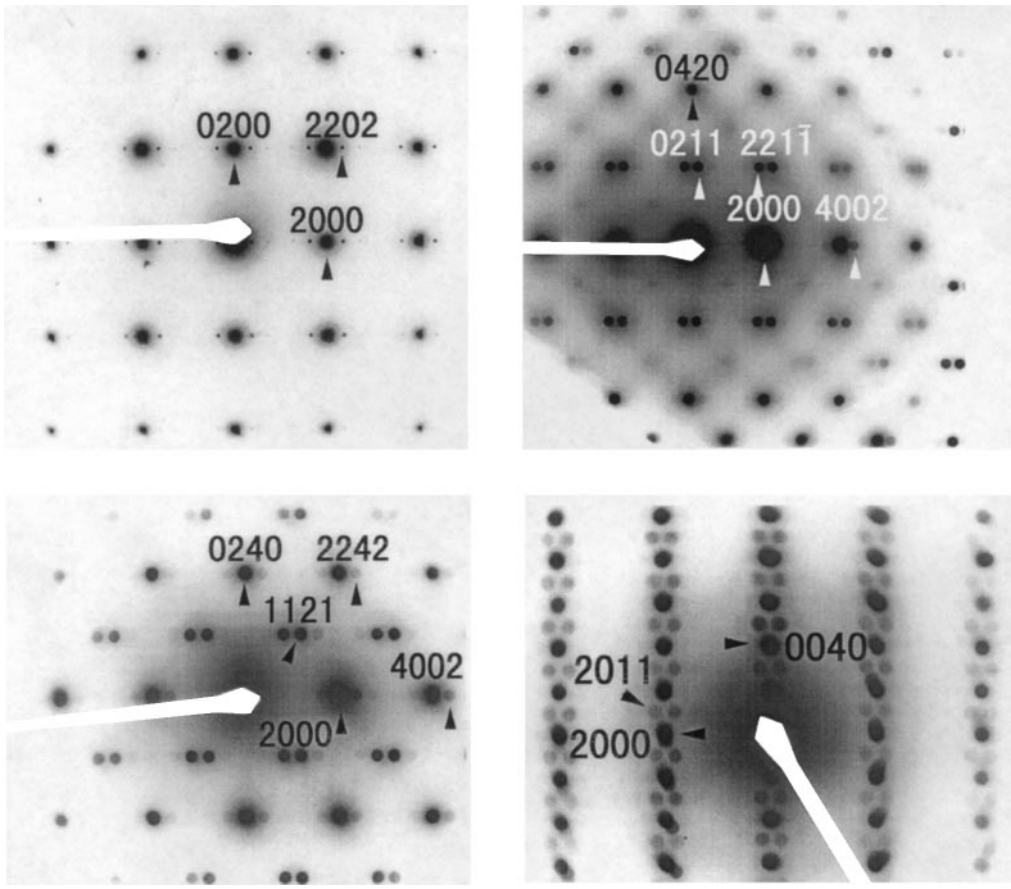

FIG. 2. (a, top left) [001], (b, top right) $\langle 0\bar{1}2\rangle$, (c, bottom left) $\langle 0\bar{2}1\rangle$ and (d, bottom right) $\langle 010\rangle$ zone axis EDPs typical of $TlCoCuSe_2$. A four-integer ([*hklm*]*) indexation scheme is used with corresponding basis vectors $M^* = \{\mathbf{a}^*, \mathbf{b}^*, \mathbf{c}^*, \mathbf{q}_i \sim 0.184\mathbf{a}^*\}$.

Systematic tilting experiments (see, for example, the $\langle 0\bar{1}2\rangle$ and $\langle 0\bar{2}1\rangle$ zone axis micro-diffraction patterns of Figs. 2b and 2c) show that the primary modulation wave vector $\mathbf{q}$ (when defined with respect to the allowed reflections of the underlying *F*-centered average structure) has a rational wave vector component, $\mathbf{q}_r = \mathbf{c}^*$, and an irrational component $\mathbf{q}_i \sim 0.184\mathbf{a}^*$ (9–12). This is confirmed by the [010] zone axis microdiffraction pattern shown in Fig. 2d. (Note that the layered nature of these phases means that grains are invariably platey with the normal oriented close to the [001] zone axis orientation making it extremely difficult to obtain orthogonal zone axis orientation EDPs such as that shown in Fig. 2d.) It is convention in such cases to redefine $\mathbf{q}$ as $\mathbf{q}_i$ (10) and to take account of the rational wave vector component via appropriate superspace centering operations (see below). In the current case, this convention requires a four-integer ([*HKLm*]*) indexation scheme (as used in Fig. 2) with corresponding basis vectors given by $\mathbf{M}^* = \{\mathbf{a}^*, \mathbf{b}^*, \mathbf{c}^*, \mathbf{q}_i \sim 0.184\mathbf{a}^*\}$.

The observed reciprocal space Bravais lattice centering conditions are then given by $F(HKLm) = 0$ unless $H + K$, $K + L + m$, $H + L + m$ are all even, requiring an *F*-centered average structure. In conjunction with *mmm* Laue symmetry, this implies a (3 + 1)-dimensional Bravais class of $mmmF(\alpha 01)$ (a nonstandard setting of Bravais class No. 18, $mmmF(10\gamma)$, in Table 9.8.3.2(a) of (10)). The additional systematic absence condition $F(HK0m) = 0$ unless *m* is even (see Fig. 2a) requires the presence of the superspace hyperglide operation $\{x_1, x_2, -x_3, x_4 + \frac{1}{2}\}$. The absence of any other systematic absence condition (see Fig. 2d) in conjunction with the *mmm* Laue symmetry implies a (3 + 1)-dimensional superspace group symmetry of $Fmmm(\alpha 01)00s$ (a nonstandard setting of superspace group No. 69.5, $Fmmm(10\gamma)s00$, in Table 9.8.3.5 of (10)). The corresponding superspace-generating operations are given by $\{x_1, x_2 + \frac{1}{2}, x_3 + \frac{1}{2}, x_4 + \frac{1}{2}\}$, $\{x_1 + \frac{1}{2}, x_2, x_3 + \frac{1}{2}, x_4 + \frac{1}{2}\}$ (for the superspace-centering operations) and $\{x_1, -x_2, -x_3, x_4 + \frac{1}{2}\}$, $\{x_1, -x_2, x_3, x_4\}$, and $\{-x_1, -x_2, -x_3, -x_4\}$ (for the rotational superspace group operations), respectively, where $\bar{x}_{4_\mu} = \mathbf{q}\cdot\mathbf{r}_\mu + t \equiv \mathbf{q}\cdot(\mathbf{r}_\mu + \mathbf{T}) + \Phi$ (10, 12, 13).

For a truly irrational α (~ 0.184 for $x = 1$, but only very weakly dependent upon *x* experimentally), the global phase parameter Φ defining the initial phases of the AMFs (see below) can be freely chosen. However, if the parameter

α "locks in" to a rational value, the parameter Φ becomes structurally significant in that it determines the conventional resultant three-dimensional space group symmetry (10–13), e.g. $C12/m1$ for $\alpha = 2/11$ ($= 0.1818$) and $\Phi = 2n/44$, $Cmm2$ for $\alpha = \frac{2}{11}$ and $\Phi = (2n+1)/44$ and $C1m1$ otherwise. The real test of incommensurability, however, is not whether α apparently coincides with rational fractions such as $\frac{2}{11}$, but rather whether or not all possible higher order harmonic satellite reflections can be observed; i.e., is there "overlap" or interaction between the modulated intensity arising from independent subcell reflections (11, 13). In the current case, such "overlap" would require the existence of measurable intensity in satellite reflections up to 11th order. While the modulation is certainly anharmonic (up to fourth-order satellite reflections are observable in Fig. 2(a) for example), on this criterion no such "overlap" exists and so $TlCoCuSe_2$ can be treated as an incommensurately modulated structure even were the exact value of α to be $\frac{2}{11}$.

4. REAL SPACE INTERPRETATION

While we have no direct experimental evidence for Co/Cu metal ion ordering being the driving force behind the observed modulation (indeed, the obtaining of such evidence is not going to be a trivial matter given their proximity in the periodic table), we nonetheless focus largely on it in what follows. There is strong circumstantial evidence that this ordering plays a dominant role since the modulation exists only when both Cu and Co ions are present in roughly equal proportions and does not exist for either ternary end member. In addition, the sharp incommensurate satellite reflections characteristic of the slow cooled specimens can be disordered into a streak along $\mathbf{a}^*$ via rapid quenching from $\sim 900^\circ$C (see Fig. 3; cf. Fig. 3a with Fig. 2b and Fig. 3b with Fig. 2c). Such an experimental observation shows directly the importance of kinetic factors, such as ionic diffusion, in the modulation and hence confirms the role of Cu/Co ordering.

Though it is beyond the scope of the current paper to fully determine the structure of the $TlCoCuSe_2$ phase, it is possible to derive symmetry-adapted generalized expressions for the Co/Cu transition metal ion ordering and associated structural relaxation responsible for the observed satellite reflections using a modulation wave approach to structural characterization (9–13).

4.1. Underlying $ThCr_2Si_2$-Related Average Structure

The underlying average structure can safely be assumed to be of (slightly orthorhombically distorted) $ThCr_2Si_2$ type, space group symmetry $Fmmm$ ($a = a_p - b_p$, $b = a_p + b_p$, $c = c_p$). There are three symmetry-independent, fully occupied average ions per unit cell: a thallium ion at $\mathbf{r}_{Tl} = 000$ (site symmetry mmm); a "mixed" transition metal ion M at

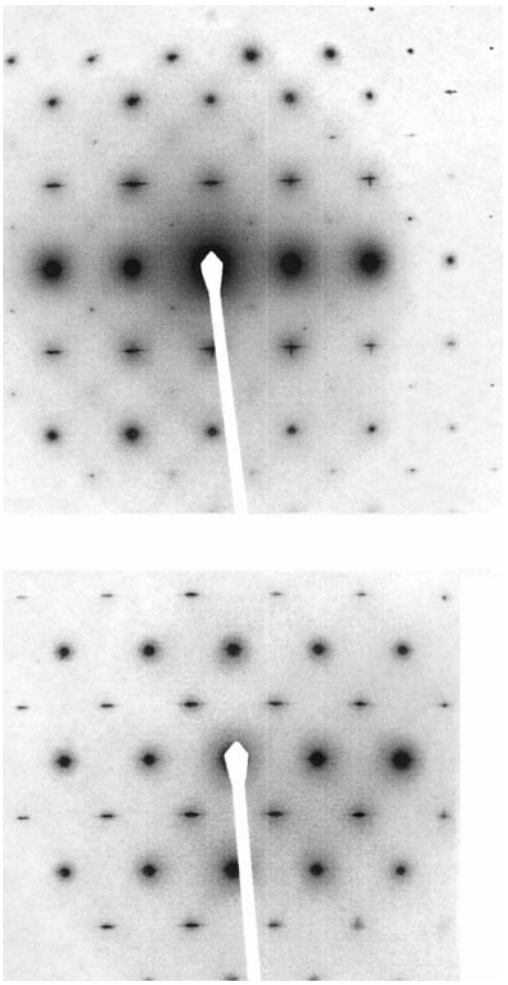

FIG. 3. (a, top) $\langle 0\bar{1}2 \rangle$ and (b, bottom) $\langle 0\bar{2}1 \rangle$ zone axis EDPs typical of disordered $TlCo_{2-x}Cu_xSe_2$ ($x \sim 1$) specimens. Note that the sharp incommensurate reflections of Fig. 2 have blurred into a continuous streak in the rapidly quenched specimens.

$\mathbf{r}_M = \frac{1}{4}, \frac{1}{4}, \frac{1}{4}$ (site symmetry 222) with an average atomic scattering factor $f_M^{av} = (1-x) f_{Co} + x f_{Cu}$, $x \sim \frac{1}{2}$; and a selenium ion at $\mathbf{r}_{Se} = 00z$ (site symmetry $mm2$) with $z \sim 0.36$ (see Fig. 4).

4.2. Atomic Modulation Functions (AMFs)

The compositional and displacive AMFs describing the perturbations away from these average occupancies and positions depend upon $(\mathbf{r}_\mu + \mathbf{T})$, i.e., the position of the μth ion (μ = Tl, Co/Cu, or Se) in the $\mathbf{T}$th ($\mathbf{T} = u\mathbf{a} + v\mathbf{b} + w\mathbf{c}$; u, v, w are integers) unit cell of the average $Fmmm$ structure (9–13) and can be written in the form

$$\delta f_\mu(\mathbf{r}_\mu + \mathbf{T}) = f_\mu^{av} \sum_m a_\mu(m) \cos\{2\pi m[\mathbf{q}\cdot(\mathbf{r}_\mu + \mathbf{T}) + \Phi] + \theta_\mu(m)\} \quad [1]$$

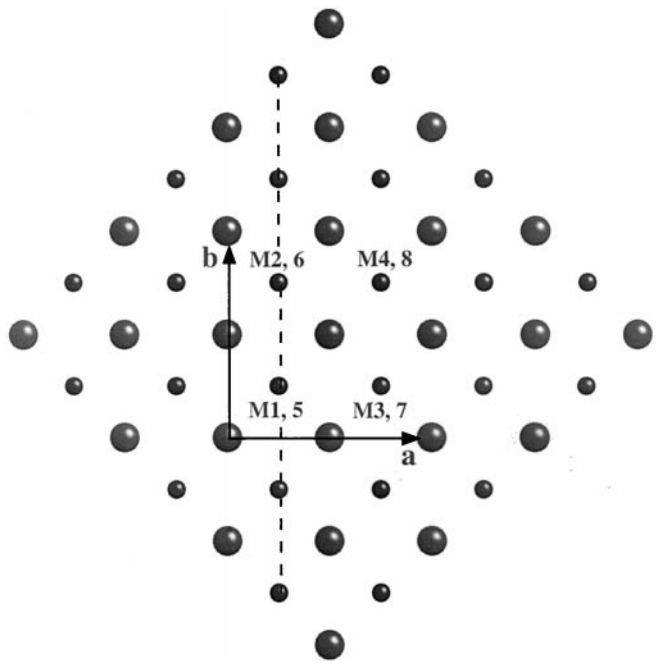

FIG. 4. Projection along [001] of the underlying *Fmmm* average structure of (slightly orthorhombically distorted) $ThCr_2Si_2$ type. The small dark balls represent the (mixed Cu/Co) *M* sites while the large balls represent the projected positions of the Tl and Se atoms. A particular one-dimensional string of *M* atom sites along *b* is shown by the dashed line. The eight *M* sites per average structure unit cell are labeled. Sites *M*5 to *M*8 are 1/2 ***c*** above the corresponding *M*1 to *M*4 sites, respectively.

and

$$\mathbf{u}_\mu(\mathbf{r}_\mu + \mathbf{T}) = \sum_{\alpha=a,b,c} \sum_m \alpha\varepsilon_{\mu\alpha}(m) \times \cos\{2\pi m[\mathbf{q}\cdot(\mathbf{r}_\mu + \mathbf{T}) + \Phi] + \theta_{\mu\alpha}(m)\} \quad [2]$$

respectively, where *m* is a positive integer and labels the particular modulation wave harmonic, and **q**, the primary modulation wave vector, is given by $\mathbf{q} \sim 0.184\mathbf{a}^*$. The modulation wave amplitudes and phases for each particular harmonic order are given by $a_\mu(m)$, $\varepsilon_{\mu\alpha}(m)$ and $\theta_\mu(m)$, $\theta_{\mu\alpha}(m)$, respectively. Keep in mind that the perpendicular space average fractional co-ordinate $\bar{x}_{4\mu} \equiv \mathbf{q}\cdot(\mathbf{r}_\mu + \mathbf{T}) + \Phi = \alpha\mathbf{a}^*\cdot(\mathbf{r}_\mu + \mathbf{T}) + \Phi$ in Eqs. [3] and [4] below is really simply a label specifying which particular average structure unit cell is being referred to (9–12).

4.3. Constraints on AMFs

The *Fmmm*(α01)00*s* superspace group symmetry can now be used to constrain the form of the above compositional and displacive AMFs, i.e., to minimize the number of independent structural variables that need to be determined in any subsequent structure refinement. Systematic application of the superspace-generating operations gives the symmetry-compatible compositional and displacive AMFs (9) as follows,

$$\delta f_M(\bar{x}_{4M})/f_M^{av} = \sum_m a_M(m)\cos\{2\pi m(\bar{x}_{4M} - \tfrac{1}{4})\} \quad [3]$$

for the compositional AMF describing the Co/Cu ion ordering and

$$\mathbf{u}_M(\bar{x}_{4M}) = \sum_m \mathbf{a}\varepsilon_{Mx}(m)\sin\{2\pi m(\bar{x}_{4M} - \tfrac{1}{4})\}$$

$$\mathbf{u}_{Tl}(\bar{x}_{4,Tl}) = \sum_{m=2n} \mathbf{a}\varepsilon_{Tl,x}(m)\sin\{2\pi m(\bar{x}_{4,Tl})\} + \sum_{m=2n+1} \mathbf{c}\varepsilon_{Tl,z}(m)\sin\{2\pi m(\bar{x}_{4,Tl})\}$$

$$\mathbf{u}_{Se}(\bar{x}_{4,Se}) = \sum_m \mathbf{a}\varepsilon_{Se,x}(m)\sin\{2\pi m(\bar{x}_{4,Se} - \tfrac{1}{4})\} + \sum_m \mathbf{c}\varepsilon_{Se,z}(m)\cos\{2\pi m(\bar{x}_{4,Se} - \tfrac{1}{4})\} \quad [4]$$

for the associated displacive AMFs, respectively.

4.4. Predicted Cu/Co Ordering Scheme

Equivalent expressions for symmetry-related atoms can also be obtained by systematic application of the above superspace-generating operations. Consider, for example, the eight *M* sites per average structure unit cell labeled *M*1 to *M*8 in Fig. 4 (sites *M*5 through *M*8 are $\frac{1}{2}c$ directly above sites *M*1 through *M*4). The analogous expressions to Eq. [3] above are

$$\delta f_{M1,2,3,4}(\mathbf{r}_{M1,2,3,4} + \mathbf{T})/f_M^{av} = \sum_m a_M(m)\cos\{2\pi m[\alpha\mathbf{a}^*\cdot(\mathbf{r}_{M1,2,3,4} + \mathbf{T}) + \Phi - \tfrac{1}{4}]\} \quad [5]$$

for *M*1 to *M*4 and

$$\delta f_{M5,6,7,8}(\mathbf{r}_{M5,6,7,8} + \mathbf{T})/f_M^{av} = \sum_m a_M(m)\cos\{2\pi m[\alpha\mathbf{a}^*\cdot(\mathbf{r}_{M5,6,7,8} + \mathbf{T}) + \Phi + \tfrac{1}{4}]\} \quad [6]$$

for *M*5 to *M*8.

Because $(\mathbf{r}_{M2} - \mathbf{r}_{M1})$, $(\mathbf{r}_{M4} - \mathbf{r}_{M3})$, etc. are parallel to *b* and orthogonal to $\mathbf{q} = \alpha\mathbf{a}^*$, the compositional AMFs will thus tend to form one-dimensional (*M*1 to *M*2 to *M*1 + *b* to … , etc.) rods or strings of *M* atoms along *b* (see the dashed line in Fig. 4) whose occupancies must all be the same; i.e., if the *M*1 site in a particular parent unit cell (**T**) happens to be occupied by a Co atom then the *M*2 site in the same parent unit cell will also be occupied by a Co atom, etc. By contrast, the compositional AMFs describing the occupancy of the *M*5 and *M*6 sites located $\frac{1}{2}c$ above the corresponding *M*1 and *M*2 sites (cf. Fig. 4 with Fig. 1) are exactly one-half a cycle out of phase with respect to the corresponding compositional AMFs of the *M*1 and *M*2 sites (cf. Eq. [5] with Eq. [6]). The physical consequences of this one-half a cycle phase shift will depend upon the exact shape of the

compositional AMF which can of course only be determined precisely from a full four-dimensional incommensurate structure refinement. It is nonetheless possible to make an informed suggestion as to the shape of this AMF on the basis of sensible crystal chemical constraints and the assumption of full (or square wave type) ordering (a reasonable assumption given the absence of the diffuse scattering which almost invariably accompanies partial ordering, cf. Fig. 2 with Fig. 3).

Given, for example, that the intensity of the observed satellite reflections (see Fig. 2) falls off rapidly with increasing harmonic order, requiring that the corresponding modulation wave amplitudes, $a_\mu(m)$ and $\varepsilon_{\mu\alpha}(m)$, must also fall off rapidly with increasing harmonic order, it is clear that the zeroth-order approximation to the shape of the compositional AMF is a simple sine wave with minima and maxima at $\bar{x}_{4M} = 0.25$ and 0.75, respectively. Given such a zeroth-order approximation to the shape of the compositional AMF, the simplest possible fully ordered form for the compositional AMF can only be a square wave function corresponding to Cu occupancy for $[\alpha\mathbf{a}^* \cdot (\mathbf{r}_M + \mathbf{T}) + \Phi]$ from 0 to $\frac{1}{2}$ and Co occupancy from $\frac{1}{2}$ to 1 (as shown in Fig. 5). Thus, if the $M1$ and $M2$ sites are occupied by Co in one particular parent unit cell (**T**), then it follows that the $M5$ and $M6$ sites in the same unit cell must be occupied by Cu and vice versa. Given an average structure c-dimension approximately midway between the significantly different c-dimensions of the two end-member parent phases, this is exactly what would be expected from a crystal chemical point of view.

Because $\alpha\mathbf{a}^* \cdot (\mathbf{r}_{M3,4} - \mathbf{r}_{M1,2}) = \frac{1}{2}\alpha$ (neighboring strings of M atoms are separated by $\frac{1}{2}$ a in the a direction; see Fig. 4), the corresponding AMFs within the same parent unit cell will also be $\frac{1}{2}\alpha \sim 0.092$ out of phase; i.e., if the $M1$ and $M2$ sites within one parent unit cell are occupied by Co then, in $100(1-\alpha) = 81.6\%$ of cases, the neighboring $M3$ and $M4$ sites will also be occupied by Co (assuming the compositional AMF shown in Fig. 5). In $100\alpha = 18.4\%$ of cases, the reverse will be true; i.e., if the $M1$ and $M2$ sites within one parent unit cell are occupied by Co then the neighbouing $M3$ and $M4$ sites will be occupied by Cu (as can be deduced from Fig. 5).

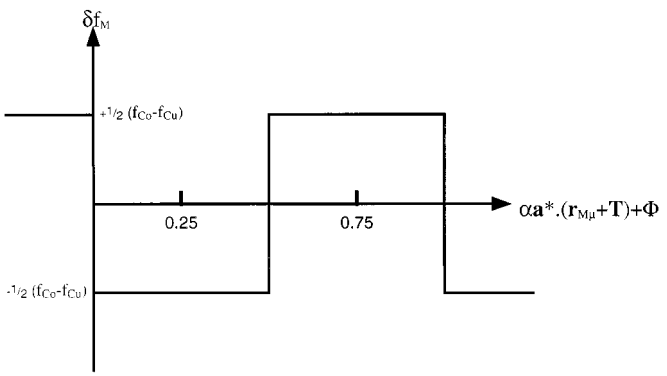

FIG. 5. Presumed square wave compositional AMF corresponding to Eq. [3] (representing the deviation of the local atomic scattering factor (composition) from the average composition of $\frac{1}{2}(f_{Co} + f_{Cu})$) plotted as a function of $\bar{x}_{4M} \equiv \alpha\mathbf{a}^*(\mathbf{r}_{M1,2,3,4} + \mathbf{T})$. Such a compositional AMF predicts Cu occupancy for $\bar{x}_{4M}$ from 0 to $\frac{1}{2}$ and Co occupancy from $\frac{1}{2}$ to 1.

Dependent upon the initial choice for Φ, the square wave compositional AMF of Fig. 5 will produce a block of either five or six neighboring strings of the same occupancy, e.g., Co followed by a block of either five or six strings of the alternative possibility, i.e., Cu, etc. The significance of the modulation wave vector magnitude α is that it determines this average block size; i.e., the average number of strings of the same composition in such a block is set by $1/\alpha = 1/0.184 = 5.44$. In many such compositionally modulated structures it has been shown that modulation wave vector magnitudes act as "chemical rulers" and can be directly related to the composition (11, 14). Such does not appear to be so in the current case.

If a five- or six-string block in one transition metal layer at $\frac{1}{4}$ c is occupied by Co, say, then the immediately neighboring block in the next layer at $\frac{3}{4}$ c will be occupied by Cu and vice-versa. Such a Co/Cu/Co $\cdots$ ordering scheme along the c direction is crystal chemically sensible in that the c dimension of $TlCoCuSe_2$ (13.70 Å) is between that of $TlCo_2Se_2$ (13.54 Å) and $TlCu_2Se_2$ (14.04 Å). One could likewise expect the height (along c) of $CuSe_4$ and $CoSe_4$ tetrahedra to be expanded and contracted relative to the average height given the parent c axis dimensions (see Eq. [4] above). On the other hand, given the similarity of the "parent" basal plane dimensions, one might not expect the average string–string separation distance to depend too much on the Co/Cu ordering scheme.

The picture that has thus emerged is that of Cu and Co atoms forming separate layers in the structure at $z = \frac{1}{4}$ and $\frac{3}{4}$, respectively, with these layers periodically interchanging as one moves along the a direction. The average interchange period is determined by $1/\alpha \sim 5.44$ neighboring strings. One possible reason for incommensurability, i.e., a non-zero α, is to minimize macroscopic strain along the a direction via the systematic alternation from one transition metal ion to the other.

Further consideration, however, is beyond the scope of the current paper and must await the results of a full four-dimensional incommensurate structure refinement.

ACKNOWLEDGMENTS

Dr. Y. Tabira is gratefully acknowledged for considerable help with production of the figures.

REFERENCES

1. G. Huan, M. Greenblatt, and M. Croft, *Eur. J. Inorg. Solid State Chem.* **26,** 193 (1989).

2. A. Newmark, G. Huan, M. Greenblatt, and M. Croft, *Solid State Commun.* **71,** 1025 (1989).
3. G. Huan and M. Greenblatt, *J. Less-Common Metals* **156,** 247–257 (1989).
4. R. Berger and C. F. van Bruggen, *J. Less-Common Metals* **99,** 113–123 (1984).
5. A. Broddefalk, P. Nordblad, and R. Berger, *Physica B*, submitted.
6. M. Oledzka, J.-G. Lee, K. V. Ramanujachary, and M. Greenblatt, *J. Solid State Chem.* **127,** 151–160 (1996).
7. R. Hoffmann and C. Zhong, *J. Phys. Chem.* **89,** 4174 (1985).
8. G. Brun, B. Gardes, J. C. Tédénac, A. Raymond, and M. Maurin, *Mater Res. Bull.* **14,** 743 (1979).
9. J. M. Pérez-Mato, G. Madariaga and M. J. Tello, *J. Phys. C* **19,** 2613–2622 (1986).
10. T. Janssen, A. Janner, A. Looijenga-Vos, and P. M. de Wolff, *in* "International Tables for Crystallography," (A. J. Wilson, Ed.), Vol. C, Kluwer, pp. 797–835, Dordrecht, 1992.
11. R. L. Withers, S. Schmid, and J. G. Thompson, *Prog Solid State Chem.* **26,** 1–96 (1998).
12. S. van Smaalen, *Cryst. Rev.* **4,** 79–202 (1995).
13. J. M. Pérez-Mato, *in* "Methods of Structural Analysis of Modulated Structures and Quasicrystals" (J. M. Pérez-Mato, F. J. Zúñiga, and G. Madariaga, Eds.), pp. 117–128, World Scientific, Singapore, 1991.
14. M. Evain, F. Boucher, O. Gourdon, V. Petricek, M. Dusek, and P. Bezdicka, *Chem. Mater.* **10,** 3068 (1998).